Terra Nova

doi: 10.1111/ter.12053

Granite emplacement by crustal boudinage: example of the Calmayo and El Hongo plutons (Córdoba, Argentina)

Fernando D'Eramo,[1] José M. Tubía,[2] Lucio Pinotti,[1] Néstor Vegas,[2] Jorge Coniglio,[1] Manuel Demartis,[1] Aitor Aranguren[2] and Miguel Basei[3]

[1]*Departamento de Geología, CONICET, FCEFQyN, Universidad Nacional de Río Cuarto, P.O. Box 3, Río Cuarto, E-5800, Argentina;* [2]*Departamento de Geodinámica, Facultad de Ciencia y Tecnología, Universidad del País Vasco (UPV/EHU), a. p. 644, Bilbao, E-48080, Spain;* [3]*Instituto de Geociências, Universidade de São Paulo, Rua do Lago 562, São Paulo, SP, Brazil*

ABSTRACT

This study deals with the structure and emplacement of the Calmayo and El Hongo trondhjemite plutons (Famatinian belt of Córdoba, Argentina). It provides structural data from the granites and the country rocks and a study of the magnetic fabric in the plutons. New U/Pb geochronological data yield intrusion ages of 512.1 ± 3.4 Ma and 500.6 ± 4.5 Ma for the Calmayo and El Hongo plutons respectively. The El Hongo massif and the southern part of the Calmayo trondhjemite preserve magmatic structures, whereas the northern domain of Calmayo shows the imprint of solid-state deformation. The main foliation in the country rocks outlines a boudin-like pattern at the map scale and the granites are located along boudin necks, suggesting that the emplacement of these trondhjemite plutons was linked to large-scale boudinage of the country rocks.

Terra Nova, 0, 1–8, 2013

Introduction

Knowledge of the structure of granite massifs has seen a remarkable improvement due to the proliferation of structural studies (Corry, 1988; Hutton, 1988; Kisters *et al*., 2009), application of gravity (Vigneresse, 1995; Améglio and Vigneresse, 1999) and magnetic susceptibility (Bouchez, 1997) methods, and the extrapolation of experimental results on the migration of granite analogues (Román-Berdiel *et al*., 1995, 2000).

Detailed information about the structural evolution of the country rocks remains essential to constrain accurately the emplacement history of a pluton, as different geological structures may be involved in the whole process leading from magma collection to the ultimate construction of granite plutons. For example, melt can be accumulated in fold hinges (Williams *et al*., 1995), and the contacts between competent and incompetent rocks can behave as barriers hindering the rise of magma and promoting its lateral spreading (Corry, 1988). However, shear zones are the most frequently described structures associated with granite emplacement. Their role is twofold: they can be used as channels for the ascent of magma, and may provide low-pressure sites where magma can be stored (Hutton *et al*., 1990; D'Lemos *et al*., 1992; Hutton and Reavy, 1992; Tikoff and Teyssier, 1992; McNulty, 1995; Brown and Solar, 1998; Weinberg *et al*., 2004).

This study deals with the emplacement of the El Hongo and Calmayo plutons, two trondhjemite bodies belonging to the Sierra Chica de Córdoba (SCC) (Argentina), and provides new U/Pb zircon ages for both plutons. The study combines structural information from the country rocks with structural and magnetic fabric data from the Calmayo and El Hongo trondhjemites. The structure of the El Hongo pluton has been published previously (D'Eramo *et al*., 2006) and will be commented briefly here. Based on such data, we propose that large-scale boudinage of the country rocks may be an efficient mechanism triggering the emplacement of granite plutons. Many authors have noticed that leucosome is observed to collect in boudin necks of deformed migmatites (Ramberg, 1955; Van der Molen, 1985; Brown, 1994; Sawyer, 1994; Brown and Rushmer, 1997; Vanderhaegue, 1999; Vanderhaeghe, 2001; Arslan *et al*., 2008), but to our knowledge, this is the first reported case of granite plutons emplaced in large-scale inter-boudin partitions.

Correspondence: José M. Tubía, Departamento de Geodinámica, Facultad de Ciencia y Tecnología, Universidad del País Vasco (UPV/EHU), a. p. 644, E-48080 Bilbao, Spain. Tel.: 00 34 946 0153 92; fax: 00 34 946 01 24 70; e-mail: jm.tubia@ehu.es

Regional frame and granite geology

The SCC belongs to the eastern Sierrras Pampeanas of the Andes and shows Palaeozoic basement, uplifted by Tertiary reverse faults, within Cretaceous and Cenozoic deposits (Fig. 1). The basement consists mainly of coarse-grained gneisses of medium-to-upper amphibolite facies, with amphibolite, granite and locally marble (Fig. 2A). In the study area, the basement includes the El Hongo, San Agustin and Calmayo trondhjemite plutons. Fig. 1 shows the location of these trondhjemite plutons in the SCC. The trondhjemite plutons of the SCC, whose intrusion ages are poorly constrained, are linked to the Famatinian subduction that started at around 500 Ma (Rapela *et al*., 1998). These authors obtained a SHRIMP U-Pb zircon age of 499 ± 6 Ma for the emplacement of the Güiraldes trondhjemite.

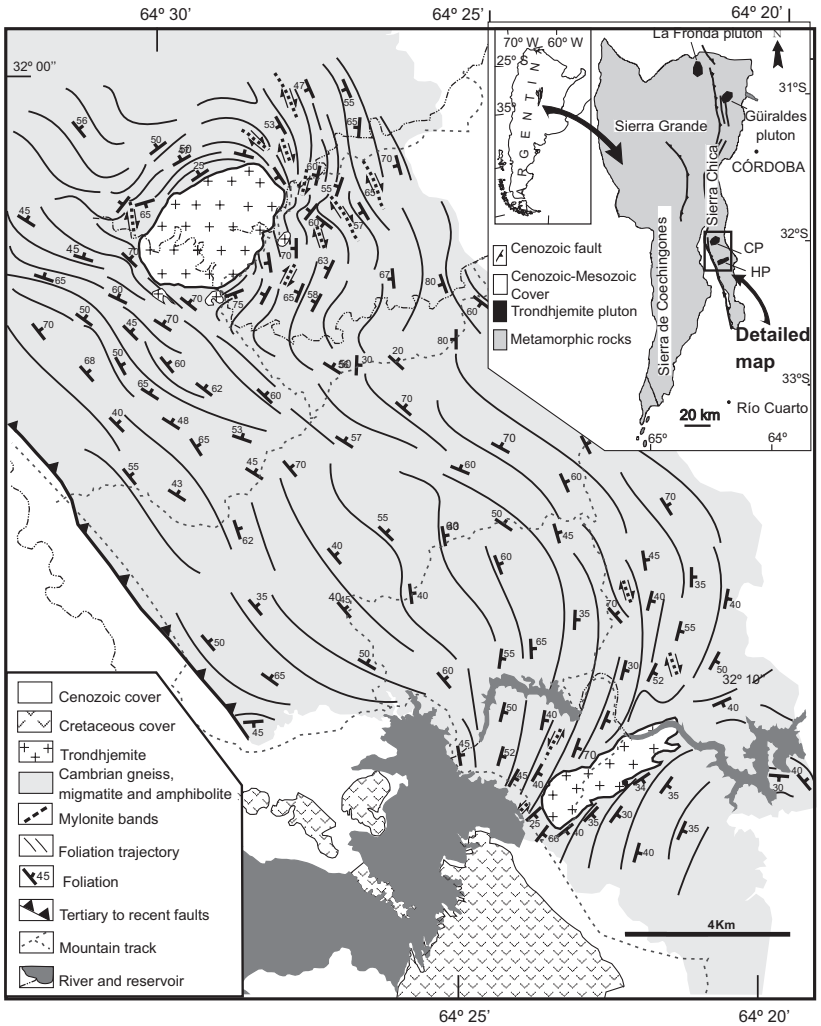

Fig. 1 Structural map of the Sierra de Chica de Córdoba around the Calmayo and El Hongo trondhjemite plutons. (Inset: location of the Calmayo (CP) and El Hongo (HP) plutons).

The Calmayo and El Hongo plutons are small, ENE–WSW elongate massifs of elliptical and rectangular shapes respectively (Fig. 1). They cut at high angle the structure of the country rocks (Fig. 1). Two main facies compose the Calmayo and El Hongo plutons. Coarse-grained, hypidiomorphic trondhjemite dominates and scarce fine-grained porphyritic facies are concentrated in the borders of each massif. The coarse-grained rocks contain more than 90% plagioclase and quartz, with biotite as the most abundant mafic mineral. Accessory minerals include epidote, apatite, magnetite, zircon and titanite. Idiomorphic epidote with allanite core is frequent as inclusions in biotite (Fig. 3A). Such a texture points to magmatic epidote, which is consistent with very low TiO_2 (≥0.015 wt%) and high pistacite contents (26.30–28.60 wt%). Magmatic epidote attests to a deep origin and fast ascent of the magma (Zen and Hammarstrom, 1984; Schmidt and Thompson, 1996). Inclusions of magnetite are frequent in biotite, as either equiaxial or extremely elongate crystals (shape ratios >10) are parallel to the (001) biotite cleavage (Fig. 3B). The fine-grained porphyritic trondhjemite, composed of plagioclase phenocrysts in a groundmass of quartz, plagioclase and biotite, suggests fast cooling at shallow crustal levels.

New U-Pb isotope analyses were carried out following the standard procedures described by Basei *et al.* (1995). Thirteen zircon fractions were analysed: seven from the Calmayo and six from the El Hongo plutons. Zircon crystals are idiomorphic with well-defined faces and edges. After data reduction, the results were plotted using the software ISOPLOT/EX (Ludwig, 1998). For the El Hongo pluton, an age of 500.6 ± 4.5 Ma and 1.3 MSWD is defined by points 2184, 2187 and especially by the more concordant fraction 2243 (Fig. 4A). Points 2198, 2200, 2202 and 2241 from the Calmayo pluton yield an age of 512.1 ± 3.4 Ma and 2.3 MSWD (Fig. 4B). These ages represent the time of zircon crystallization and granite emplacement. For both samples, the scattering of the remaining points suggests recent lead loss. The emplacement age of 500.6 ± 4.5 Ma for the El Hongo pluton agrees with the age of the Güiraldes trondhjemite (Rapela *et al.*, 1998), whereas the Calmayo pluton is a bit older, 512.1 ± 3.4 Ma.

Field structural data

The dominant structure of the basement is a NE-dipping foliation parallel to the axial surface of tight folds. The presence of garnet, plagioclase and cordierite porphyroblasts gives a wavy appearance to the gneissic foliation (Fig. 2B). The foliation in the country rocks shows a dominant NW–SE strike and dips steeply to the NE (Fig. 1), reflecting a bulk NE–SW shortening consistent with the widespread presence of boudins and pinch-and-swell structures (Fig. 2C). Boudins display steep-plunging necks or sub-horizontal and NW-trending necks in nearby outcrops. The foliation trajectories outline a boudin-like geometry (Fig. 1). They also draw triple points around the Calmayo pluton, suggesting that the shortening was active after its emplacement.

Late shear bands with S-C mylonites appear locally (Fig. 2D). They dip 50°–70° SW and strike NNW except close to the Calmayo and El Hongo plutons, where they display N–S or NE–SW strikes (Fig. 1B). Whatever their strike, they yield reverse motions with a minor dextral component, except along a few

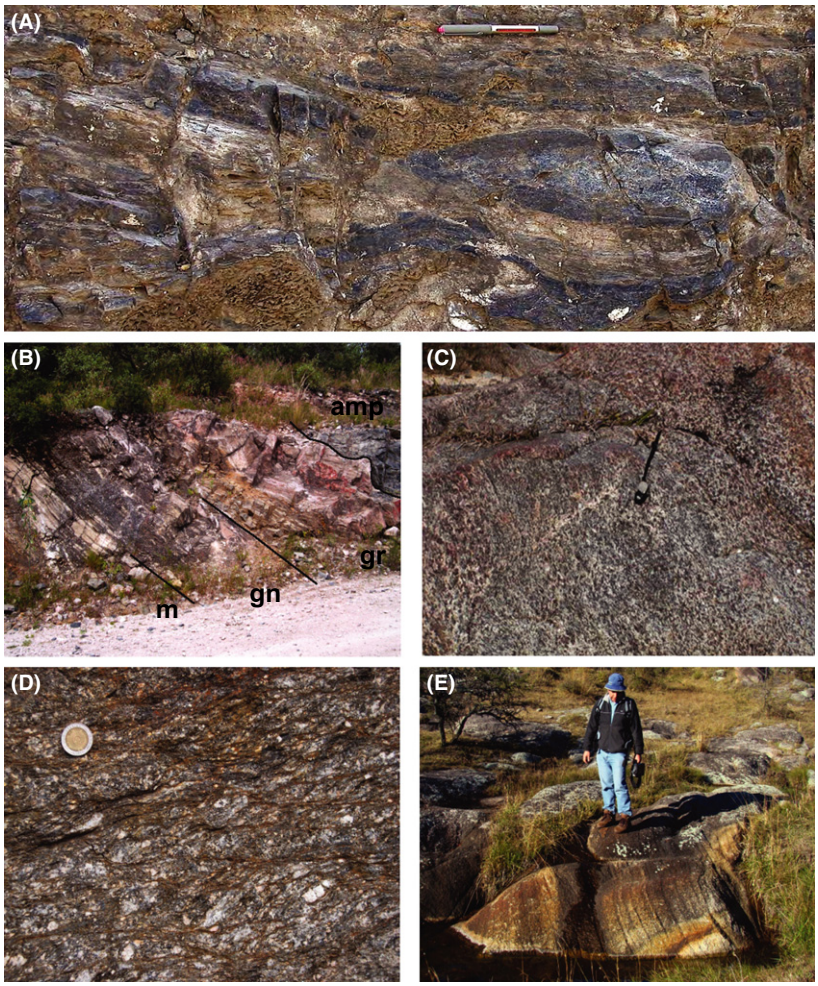

Fig. 2 Field aspect and structures of the Calmayo trondhjemite and its country rocks. (A) Inter-layered amphibolite (amp), granite (gr), gneiss (gn) and marble (m). (B) Aspect of the main foliation in the dominant gneissic rocks of the country rock sequence. (C) Boudins in an amphibolite layer surrounded by gneiss. (D) S-C structures related to late shear bands in the country rocks. (E) Magmatic layering in the Calmayo pluton.

ENE-striking shear zones located close to the Calmayo pluton where sinistral displacements are observed. These shear bands are linked to the Soconcho belt, a SW-dipping reverse shear zone, which extends more than 35 km along the southern part of the SCC (Martino *et al.*, 1995).

Two types of planar structures of magmatic origin are recognized within the Calmayo and El Hongo plutons: (i) a magmatic layering, defined by thin biotite-rich bands alternating with thicker plagioclase- and quartz-bearing layers (Fig. 2E); and (ii) a foliation defined by the parallel arrangement of the plagioclase and biotite. The magmatic origin of the foliation is evidenced because these minerals coexist with equiaxial aggregates of quartz devoid of solid-state deformation microstructures. The layering and the magmatic foliation are parallel and show westward dips and N- to NNW-strike. These structures display similar orientation in both massifs.

The Calmayo pluton shows two structural domains. Magmatic structures are widespread to the south and solid-state deformation structures are observed in its north-eastern corner. The solid-state deformation led to S/C structures, consistent with the motion of the Soconcho shear zone.

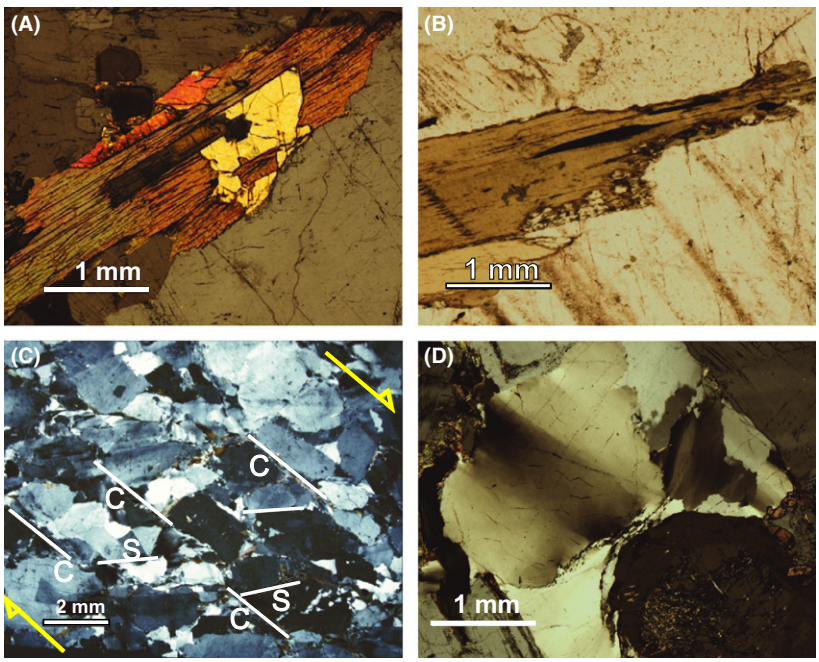

Fig. 3 Photomicrographs from the Calmayo trondhjemite. (A) Magmatic epidote (ep) hosted by biotite. (B) elongate inclusions of magnetite in biotite. (C) S-C microstructures with dextral shear sense from the NE-portion of the pluton. (D) Sub-grain boundaries with perpendicular orientation in quartz. The small, new recrystallized grains of quartz are consistent with low-temperature of deformation.

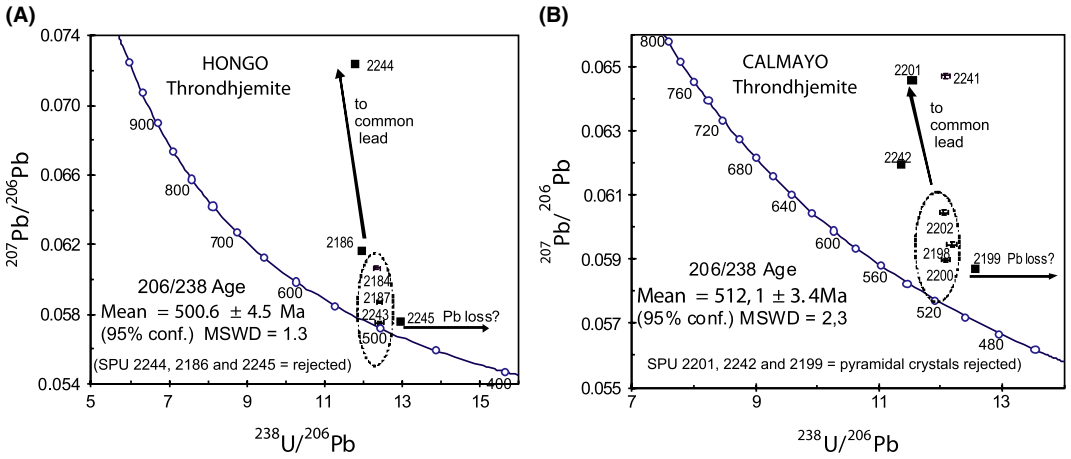

Fig. 4 Tera-Wasserburg diagrams for the El Hongo and Calmayo trondhjemites.

The spacing between C-planes (>2 cm) and the C-S angles (≈40°) (Fig. 3C) point to a weak deformation (Berthé *et al.*, 1979; Dell'Angelo and Tullis, 1989). In the NE corner, a WNW-trending stretching lineation is defined on by elongate aggregates of quartz. The grains of quartz present sub-grain boundaries and small new grains pointing to low-temperature conditions during deformation. The sub-grain boundaries are usually arranged in two nearly perpendicular systems symmetrical with respect to the foliation trace (Fig. 3D), which is consistent with a weak rotational deformation (Bouchez and Duval, 1982).

Magnetic fabric in the Calmayo pluton

Anisotropy of the magnetic susceptibility (ASM) has been analysed on samples from 26 sites from the Calmayo pluton. Two or three oriented cores per site were extracted with a portable drilling machine, and three cylindrical samples (24 mm in diameter and 22 mm high) were obtained from each core, affording 213 specimens. Measurements were performed at the UPV/EHU, using a Kappabridge KLY-2 bridge (Geofysica, Brno), yielding magnetic susceptibility values and orientations of the three principal axes of the AMS ellipsoids ($K_1 > K_2 > K_3$). The bulk susceptibility, K, is expressed as $(K_1 + K_2 + K_3)/3$. The magnetic lineation corresponds to the K_1-axis and the K_3-axis determines the pole to the foliation. The principal anisotropy parameters are given as $P = K_1/K_3$ or the corrected anisotropy degree (Jelinek, 1981), $Pj = \exp\sqrt{\{2[(\eta_1 - \eta_m)^2 + (\eta_2 - \eta_m^2)^2 + (\eta_3 - \eta_m)^2]\}}$, where: $\eta_1 = \ln K_1$, $\eta_2 = \ln K_2$, $\eta_3 = \ln K_3$ and $\eta_m = (\eta_1 + \eta_2 + \eta_3)/3$. The eccentricity of the magnetic ellipsoid is expressed by the shape parameter (Jelinek, 1981), $T = [2 \ln (K_2/K_3)/\ln (K_1/K_3) - 1]$.

K varies from 45 μSI to 4770 μSI (Fig. 5A). Nine sites provide K-values lower than 300 μSI, typical of paramagnetic granitoids; their AMS mainly reflect the orientation of biotite and amphibole in the rock. K-values greater than 300 μSI (60% of sites) indicate that magnetite makes a significant contribution to susceptibility and usually to the anisotropy, their AMS reflecting the shape fabric of magnetite (Rochette, 1987; Bouchez, 1997). The magnetic phases have been determined measuring K as a function of temperature in a CS-2 furnace coupled to the Kappabridge (Fig. 5B). The analysed

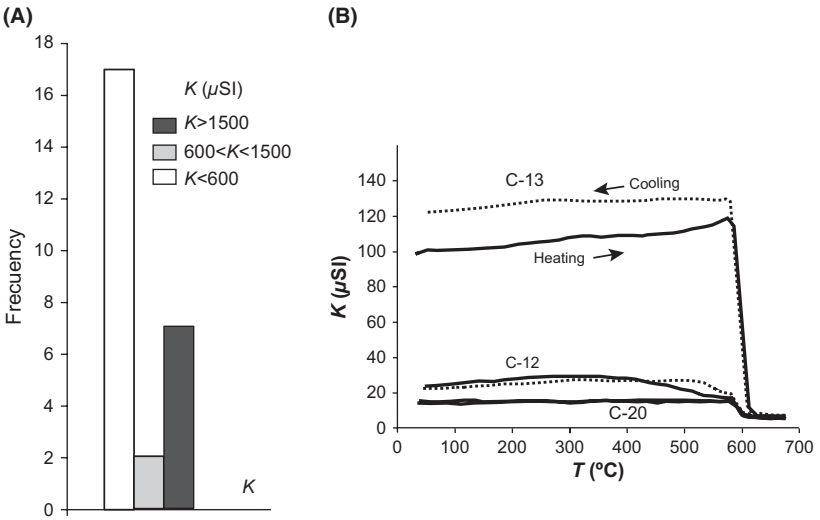

Fig. 5 Magnetic susceptibility characteristics of the Calmayo pluton. (A) Histogram showing distribution of the magnetic susceptibility values. (B) Temperature dependence of magnetic susceptibility in samples having different susceptibility values. The magnetic susceptibility values have not been normalized to the volume of powder and, therefore, are much lower than those of the corresponding solid core specimen.

samples correspond to small amounts (0.25 cm^3) of crushed samples and cover the whole range of *K*-values found in the Calmayo pluton. The heating runs reveal the presence of magnetite in all three samples, as indicated by the susceptibility drop at ~580 °C, the Curie temperature for this mineral. The magnetic anisotropy and susceptibility show a direct correlation, as P increases as *K* does (Fig. 6A). *T*-values fluctuate between −0.63 and 0.82, with a mean value of 0.33 and most sites provide oblate magnetic fabrics (Fig. 6B).

The magnetic foliation strikes NNW–SSE to N–S and dips steeply to the west in the two plutons (Fig. 7). Field and magnetic foliation measurements give similar results, a fact pointing to biotite as the main marker of the shape fabric in granites even if magnetite is dominant, as this mineral has a mimetic fabric (Grégoire *et al.*, 1998); elongate magnetite inclusions parallel to the (001) cleavage of host biotite crystals (Fig. 3B) support this interpretation. Moreover, the concordance between the magnetic and field fabrics points to magnetic anisotropy triggered by multi-domain magnetite, as single-domain magnetite would result in inverse magnetic fabrics (Tarling and Hrouda, 1993). In the Calmayo pluton, the magnetic lineation differentiates two structural domains: S-plunging lineations dominate in the SW part of the massif, whereas WNW-plunging lineations prevail in the NE zone (Fig. 7). The WNW-trending lineations proceed from outcrops showing solid-state deformation, suggesting that the magmatic foliation was reactivated as shear planes during the late shearing, whereas the magmatic lineation was replaced by a stretching lineation.

Discussion and conclusions

Petrographical, geochemical and age affinities between the El Hongo and Calmayo plutons point to magma emplacement from a common magmatic source during the same tectonic event of the Famatinian cycle. Steep-dipping foliations are observed all over these plutons (Fig. 7). We attribute this structural homogeneity

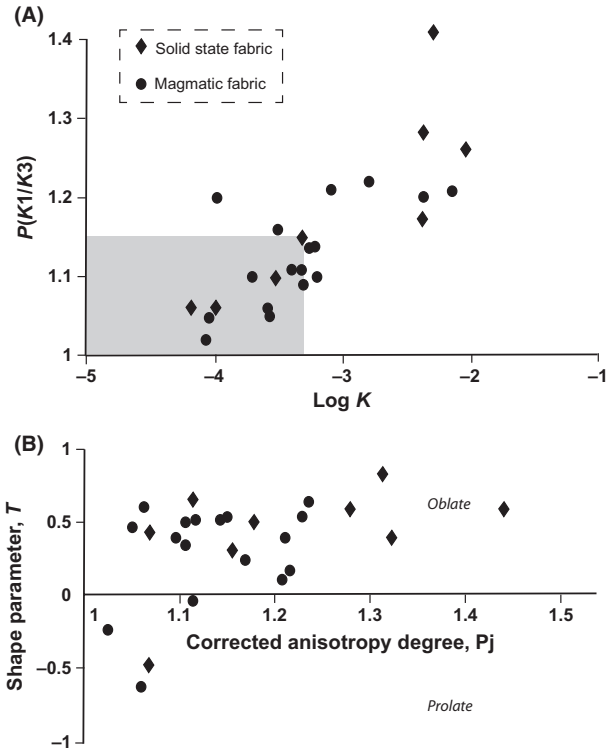

Fig. 6 Magnetic anisotropy characteristics of the Calmayo pluton. (A) Magnetic anisotropy, *P*, vs. magnetic susceptibility, *K*. There is a direct correlation between *P*- and *K*-values. Shaded area: domain of paramagnetic granites. (B) Shape parameter, *T*, vs. corrected anisotropy, Pj. Oblate fabrics predominate.

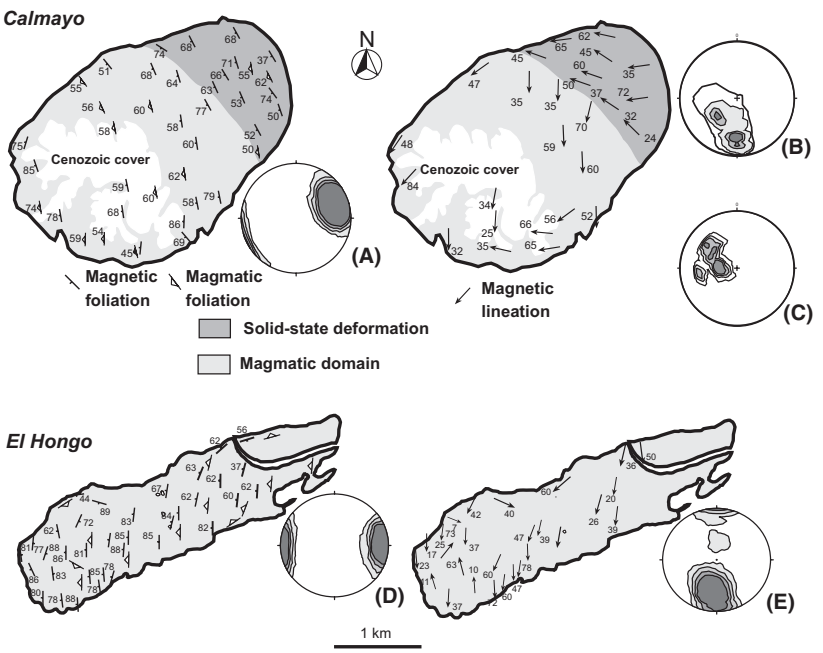

Fig. 7 Foliation and lineation maps in the Calmayo and EL Hongo plutons. Steroplot of poles to the magnetic foliation in the Calmayo (A) and El Hongo (D) plutons. Stereoplots of lineations in the magmatic (B) and solid-state deformation (C) domains from the Calmayo pluton and in the El Hongo (E) pluton.

to the current erosional level of granite sheets with flat roof and basal contacts, as shown in the cross-section through the Calmayo pluton (Fig. 8). Such geometry agrees with the gravity-constrained shape of the El Hongo pluton (D'Eramo *et al.*, 2006), corresponding to a very thin horizontal sheet resting on two N-trending root zones (Fig. 9B). Besides, a thickness of only 0.8 km results for the Calmayo pluton from the length-to-thickness relationship proposed by Petford *et al.* (2000). We tentatively place the last magmatic pulse towards the northern side of the Calmayo pluton. Such a location would give an explanation to the localization of solid-state deformation in that part, which resting confined between, and being weaker than, the fully crystallized granite to the SW and the country rocks to the NE could promote a brittle–ductile deformation during the last events of regional shortening.

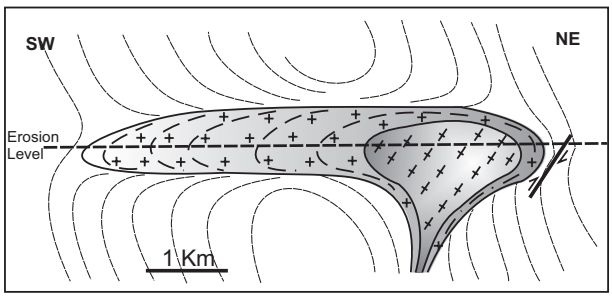

Fig. 8 Schematic NE–SW cross-section of the Calmayo pluton.

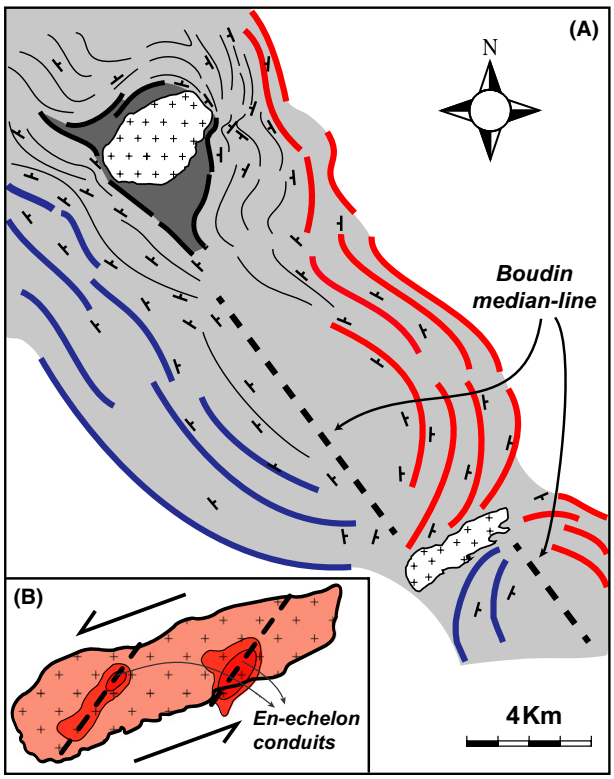

Fig. 9 (A) Sketch showing a boudin-like structure at the map scale and the location of the trondhjemite plutons in inter-boudin partitions. The red and blue lines mark the eastern and western edges of the boudins respectively. The dark grey colour outlines foliation triple points around the Calmayo plutons. Close to the El Hongo pluton, a sinistral displacement along the inter-boudin partition zone is evidenced when the boudin median-lines are taken as reference. (B) The same shear sense can be deduced from *en-échelon* conduits revealed by two negative gravity anomalies located below the El Hongo pluton (modified after D'Eramo *et al.*, 2006).

The foliation trajectories bring to light an asymmetric boudin-like structure in the country rocks of the Calmayo and El Hongo plutons (Fig. 9). A cursory glance at the foliation map could lead to the misleading conclusion that the deflection of foliation around the El Hongo pluton is due to dextral shearing. However, a sinistral displacement along the inter-boudin partition zone is evidenced when the boudin median-lines are taken as reference (Fig. 9A). This shear sense is also supported by two negative gravity anomalies located below the El Hongo pluton, compatible with *en-échelon* fractures linked to sinistral shearing (Fig. 9B) and interpreted as feeder magma conduits (D'Eramo *et al.*, 2006). Therefore, the opposite deflections of the foliation do not imply a dextral shear zone, but they rather correspond to the eastern and western edges of neighbour boudins brought in contact after the sinistral motion (Fig. 9A).

We interpret the boudin-like structure of the Calmayo and El Hongo country rocks as a case of foliation boudinage at crustal scale. Foliation boudinage was first described in Swiss glaciers to account for the formation of boudin-like structures in compositionally homogeneous glace with a strong planar anisotropy (Hambrey and Milnes, 1975). Similar structures have been recognized in metamorphic rocks with no lithology contrast (Platt and Vissers, 1980; Lacassin, 1988; Arslan *et al.*, 2008). For our interpretation to be correct, the metamorphic basement should react to the NE–SW shortening like a homogeneous sheet. We consider that the country rocks meet this condition at the megascopic scale, even if they show variances at outcrop scale, as the size of this boudin-like structure is at least three orders of magnitude thicker than the layers composing the metamorphic basement (compare Figs 2B and 9A). The migration of melts to boudin necks has been long recognized in migmatite domains,

but to our knowledge, this is the first example of granite emplacement by boudinage processes at crustal scale.

Acknowledgements

We acknowledge the comments of three anonymous reviewers: Agencia de Promoción Científica y Técnica, SeCyT Universidad Río Cuarto (PICT-2008-1477 and program 18/C 360) and CONICET (PIP-CONICET-0916). Analytical data were financed by CGL2010-14869, CGL2011-23755 (Minsterio de Ciencia e Innovación, Spain) and IT-364-10 (Gobierno Vasco) Spanish projects.

References

Améglio, L. and Vigneresse, J.L., 1999. Geophysical imaging of the shape of granitic intrusions at depth: a review. In: *Understanding Granites: Integrating New and Classical Techniques* (A. Castro, C. Fernández and J.L. Vigneresse, eds). *Spec. Publ. Geol. Soc. Lond.*, **168**, 39–54.

Arslan, A., Passchier, C.W. and Koehn, D., 2008. Foliation boudinage. *J. Struct. Geol.*, **30**, 291–309.

Basei, M.A.S., Siga Junior, O., Sato, K. and Sproesser, W.M., 1995. A instalação da metodologia U-Pb na Universidade de São Paulo. Princípios metodológicos, aplicações e resultados obtidos. *An. Acad. Bras. Ciencias*, **67**, 221–236.

Berthé, D., Choukroune, P. and Jegouzo, P., 1979. Orthogneiss, mylonite and non coaxial deformation of granites: the example of the South Armorican Shear Zone. *J. Struct. Geol.*, **1**, 31–42.

Bouchez, J.L., 1997. Granite is never isotropic: an introduction to ASM studies of granitic rocks. In: *Granite: From Segregation of Melt to Emplacement Fabrics (Petrology and Structural Geology)* (J.L. Bouchez, D.H.W. Hutton and W.E. Stephens, eds). pp. 95–112. Kluwer, Dordrecht.

Bouchez, J.L. and Duval, P., 1982. The fabric of polycrystalline ice deformed in simple shear: experiments in torsion, natural deformation and geometrical interpretation. *Text. and Microstruc.*, **5**, 171–190.

Brown, M., 1994. The generation, segregation, ascent and emplacement of granite magma: the migmatite-to-crustally-derived granite connection in thickened orogens. *Earth-Sci. Rev.*, **36**, 83–130.

Brown, M. and Rushmer, T., 1997. The role of deformation in the movement of granitic melt: views from the laboratory and the field. In: *Deformation-enhanced Fluid Transport in the Earth's Crust and Mantle* (M.B. Holness, ed.), pp. 111–144. Chapman and Hall, London.

Brown, M. and Solar, G.S., 1998. Granite ascent and emplacement during contractional deformation in convergent orogens. *J. Struct. Geol.*, **20**, 1365–1393.

Corry, C.E., 1988. Laccoliths: mechanics of emplacement and growth. *Geol. Soc. Am. Spec. Pap.*, **220**, I–110.

Dell'Angelo, L.N. and Tullis, J., 1989. Fabric development in experimentally sheared quartzites. *Tectonophysics*, **169**, 1–21.

D'Eramo, F.J., Pinotti, L.P., Tubía, J.M., Vegas, N., Coniglio, J., Aranguren, A., Tejero, R. and y Gómez, D., 2006. Coalescence of lateral spreading magma ascending through dykes: a mechanism to form a granite canopy (El Hongo pluton, Sierras Pampeanas, Argentina). *J. Geol. Soc. London*, **163**, 881–892.

D'Lemos, R.S., Brown, M. and Strachan, R.A., 1992. Granite magma generation, ascent and emplacement within a transpressional orogen. *J. Geol. Soc. London*, **149**, 487–490.

Grégoire, V., Darrozes, J., Gaillot, P. and Nédélec, A., 1998. Magnetite grain shape fabric and distribution anisotropy vs rock magnetic fabric: a three-dimensional case study. *J. Struct. Geol.*, **20**, 937–944.

Hambrey, M.J. and Milnes, A.G., 1975. Boudinage in glacier ice–some examples. *J. Glaciol.*, **14**, 383–393.

Hutton, D.H.W., 1988. Granite emplacement mechanisms and tectonic controls: inferences from deformation studies. *Trans. R. Soc. Edinb. Earth Sci.*, **79**, 245–255.

Hutton, D.H.W. and Reavy, R.J., 1992. Strike-slip tectonics and granite emplacement. *Tectonics*, **11**, 960–967.

Hutton, D.H.W., Depster, T.J., Brown, P.E. and Becker, S.D., 1990. A new mechanism of granite emplacement: intrusion in active extensional shear zones. *Nature*, **343**, 452–455.

Jelinek, V., 1981. Characterization of the magnetic fabric of rocks. *Tectonophysics*, **79**, 63–67.

Kisters, A.F.M., Ward, R.A., Anthonissen, C.J. and Vietze, M.E., 2009. Melt segregation and far-field melt transfer in the mid-crust. *J. Geol. Soc.*, **166**, 905–918.

Lacassin, R., 1988. Large-scale foliation boudinage in gneisses. *J. Struct. Geol.*, **10**, 643–647.

Ludwig, K.R., 1998. *Using Isoplot/Ex. A Geochronological Toolkit for Microsoft Excel*. Berkeley Geochronology Center, Special Publication N 1. Berkeley.

Martino, R., Kraemer, P., Escayola, M., Giambastiani, M. and Arnosio, M., 1995. Transecta de las sierras Pampeanas de Córdoba a los 32° LS. *Revista de la Asociación geológica Argentina*, **50**, 60–77.

McNulty, B.A., 1995. Shear zone development during magmatic arc construction: the Bench Canyon shear zone, central Sierra Nevada, California. *Geol. Soc. Am. Bull.*, **107**, 1094–1107.

Petford, N., Cruden, A.R., McCaffrey, K.J.W. and Vigneresse, J.L., 2000. Dynamics of granitic magma formation, transport and emplacement in the Earth's crust. *Nature*, **408**, 669–673.

Platt, J.P. and Vissers, R.L.M., 1980. Extensional structures in anisotropic rocks. *J. Struct. Geol.*, **2**, 397–410.

Ramberg, H., 1955. Natural and experimental boudinage and pinch-and-swell structures. *J. Geol.*, **63**, 512–526.

Rapela, C.W., Pankhurst, R.J., Casquet, C., Baldo, E., Saavedra, J., Galindo, C. and Fanning, C.M., 1998. The Pampean orogeny of the southern proto-Andes: Cambrian continental collision in the Sierras de Córdoba. In: *The Proto-Andean Margin of Gondwana* (R.J. Pankhurst and C.W. Rapela, eds). *Spec. Publ. Geol. Soc. Lond.*, **142**, 181–218.

Rochette, P., 1987. Magnetic susceptibility of the rock matrix related to magnetic fabric studies. *J. Struct. Geol.*, **9**, 1015–1020.

Román-Berdiel, T., Aranguren, A., Cuevas, J., Tubía, J.M., Gapais, D. and Brun, J.P., 2000. Experiments on granite intrusion in transtension. In: *Salt, Shale and Igneous Diapirs in and Around Europe* (B. Vendeville, Y. Mart and J.L. Vigneresse, eds). *Spec. Publ. Geol. Soc. Lond.*, **174**, 21–42.

Román-Berdiel, T., Brun, J.P. and Gapais, D., 1995. Analogue models of laccoliths formation. *J. Struct. Geol.*, **17**, 1337–1346.

Sawyer, E.W., 1994. Melt segregation in the continental crust. *Geology*, **22**, 1019–1022.

Schmidt, M.W. and Thompson, A.B., 1996. Epidote in calc-alkaline magmas: an experimental study of stability, phase relations and the role of epidote in magmatic evolution. *Am. Mineral.*, **81**, 424–474.

Tarling, D.H. and Hrouda, F., 1993. *The Magnetic Anisotropy of Rocks*. Chapman and Hall, London. 217pp.

Tikoff, B. and Teyssier, C., 1992. Crustal-scale, en-echelon "P-shear" tensional bridges: a possible solution to the batholithic room problem. *Geology*, **20**, 927–930.

Van der Molen, I., 1985. Interlayer material transport during layer-normal shortening, II: boudinage, pinch-and-swell and migmatite at Søndre Strømfjord Airport, west Greenland. *Tectonophysics*, **115**, 275–295.
Vanderhaeghe, O., 2001. Melt segregation, pervasive melt migration and magma mobility in the continental crust: the structural record from pores to orogens. *Phys. Chem. Earth Part A.*, **26**, 213–223.
Vanderhaegue, O., 1999. Pervasive melt migration from migmatites to leucogranite in the Shuswap metamorphic core complex, Canada: control of regional deformation. *Tectonophysics*, **312**, 35–55.
Vigneresse, J.L., 1995. Crustal regime of deformation and ascent of granitic magma. *Tectonophysics*, **249**, 187–202.
Weinberg, R.F., Sial, A.N. and Mariano, G., 2004. Close spatial relationship between plutons and shear zones. *Geology*, **32**, 377–380.
Williams, M.L., Hanmer, S., Kopf, C. and Darrach, M., 1995. Syntectonic generation and segregation of tonalitic melts from amphibolite dikes in the lower crust Striding-Athabasca mylonite zone, northern Saskatchewan. *J. Geophys. Res.*, **100**, 15717–15734.
Zen, E-A. and Hammarstrom, J.M., 1984. Magmatic epidote and its petrologic significance. *Geology*, **12**, 515–518.

Received 8 February 2012; revised version accepted 19 April 2013

Supporting Information

Additional Supporting Information may be found in the online version of this article:

Table S1. AMS parameters of the Calmayo pluton.

